Earth and Planetary Science Letters 534 (2020) 116073

Contents lists available at ScienceDirect

Earth and Planetary Science Letters

www.elsevier.com/locate/epsl

Sulfur isotope characterization of primordial and recycled sources feeding the Samoan mantle plume

James W. Dottin III [a,*], Jabrane Labidi [c], Vedran Lekic [a], Matthew G. Jackson [d], James Farquhar [a,b]

[a] Department of Geology, University of Maryland, College Park, MD 20742, United States
[b] Earth System Science Interdisciplinary Center, College Park, MD 201742, United States
[c] Université de Paris, Institut de physique du globe de Paris, CNRS, F-75005 Paris, France
[d] Department of Earth Science, University of California, Santa Barbara, CA 93106, United States

ARTICLE INFO

Article history:
Received 9 May 2019
Received in revised form 20 December 2019
Accepted 6 January 2020
Available online xxxx
Editor: T.A. Mather

Keywords:
Samoa
sulfur isotopes
primordial reservoir
recycling

ABSTRACT

Understanding present-day mantle heterogeneity is key to understanding the geochemical evolution of our planet. The Samoan islands are the type locality for the Enriched Mantle (II) reservoir that is thought to be produced from the subduction and recycling of marine sediment from upper continental crust. In addition to hosting extreme radiogenic isotope compositions from the EM II reservoir, Samoa also exhibits contributions from other mantle reservoirs in a dilute form including the EM (I) (recycled continental material), HIMU (recycled oceanic crust), and DMM (depleted upper mantle) mantle reservoirs. The plume system feeding the Samoan islands sits above a seismically imaged Large Low Shear Velocity Province (LLSVP) and an Ultra-Low Velocity Zone (ULVZ) that is thought to contribute, in addition to recycled components, the recently discovered early-formed (primordial) components with negative μ^{182}W and high ^{3}He/^{4}He. Recent work measuring sulfur isotopes in ocean island basalts has established that recycled oceanic and continental crust host unique S-isotope compositions that can be identified at various hotspot localities. Here we document previously unknown relationships between Δ^{33}S and radiogenic tungsten, helium and lead isotopes from 7 Samoan basalts (from the islands of Ofu, Vailulu'u and Malumalu) that suggest mixing between several endmembers. One, a HIMU influence that has slight positive Δ^{33}S and positive δ^{34}S; another, related to EM II that has near zero Δ^{33}S and positive δ^{34}S; a third, which is primordial with negative μ^{182}W, high ^{3}He/^{4}He, that has $\Delta^{33}S = 0$ and negative δ^{34}S. From this, we conclude that the indistinguishable Δ^{33}S of the primordial endmember from that of the convective mantle indicates that sulfur isotopes were homogenized early in Earth's history. The Vailulu'u sample with HIMU characteristics, carries a small but resolvable Δ^{33}S that allows, but does not require mass-independent Archean Δ^{33}S to shift the Δ^{33}S. The observed correlations involving Δ^{33}S support arguments linking Pb, He, and W geochemistry to a deep mantle process and places constraints on questions related to the sources of mantle geochemical heterogeneity.

1. Introduction

Basalts erupted at ocean islands (OIBs) are thought to sample both the deep and convective mantle, and provide insight into the diversity of mantle reservoirs. Long-lived radiogenic isotope compositions of strontium (Sr), neodymium (Nd), and lead (Pb) from OIBs reveal compositional heterogeneity of the mantle and have formed the basis for identifying distinct mantle reservoirs produced by melt removal and incorporation of recycled components over time (Zindler and Hart, 1986). The process of core formation and further planetary differentiation allowed for the production of an early formed reservoir (from here forward in this paper, we refer to this as a *primordial* reservoir). Components of this reservoir are observed in modern mantle plume basalts such as Samoa, and are manifested as isotopic anomalies in the short lived radiogenic isotope composition of tungsten (W) (Mundl-Petermeier et al., 2019, 2020; Mundl et al., 2017; Rizo et al., 2016; also see Kruijer and Kleine, 2018) and noble gas signatures of helium (He), neon (Ne), xenon (Xe), and argon (Ar) (e.g. Kurz et al., 2009; Mukhopadhyay, 2012). The isotopic observations that iden-

* Corresponding author.
E-mail address: jdottin@umd.edu (J.W. Dottin).

https://doi.org/10.1016/j.epsl.2020.116073
0012-821X/

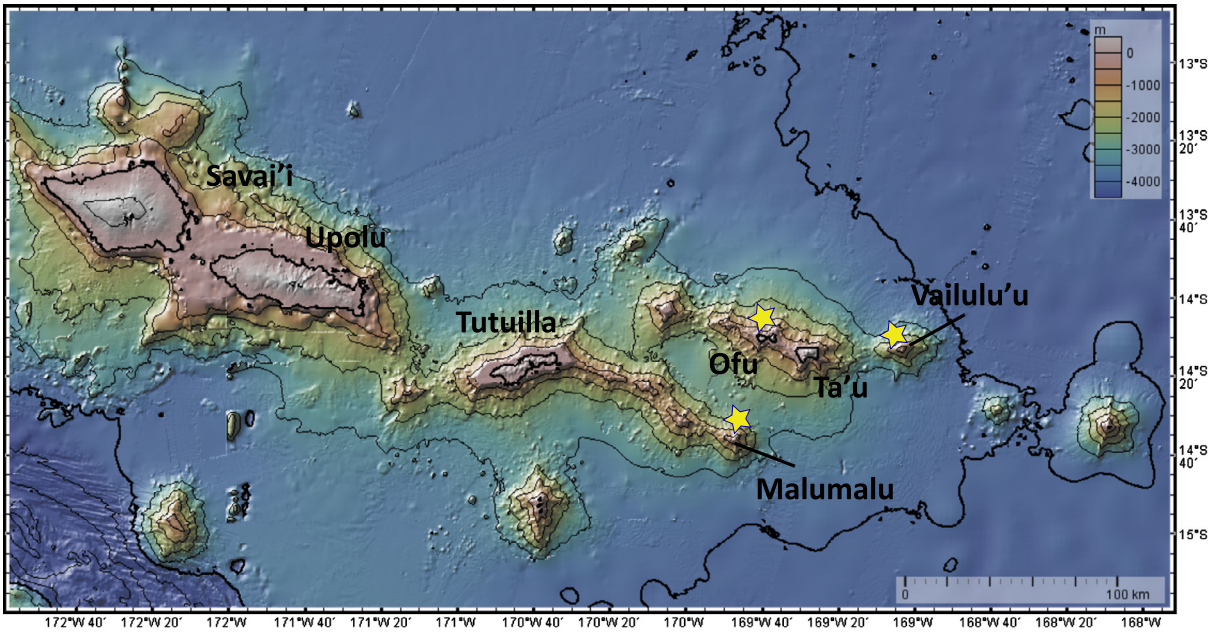

Fig. 1. Shown is a map of the Samoan volcanoes. Gold stars denote the localities sampled for this study. The map was configured using the GeoMapApp program.

tify primordial components in mantle plume systems have suggested links to Large Low Shear Velocity Provinces (LLSVPs) and Ultra Low Velocity Zones (ULVZs) in the deep mantle (Williams et al., 2019).

Here, we present new bulk rock quadruple sulfur isotope data on ($n = 7$) basalts from three Samoan volcanoes–Ofu, Vailulu'u and Malumalu (Fig. 1)–to explore whether sulfur isotopes provide insight into the primordial signatures described above. So far sulfur isotopes have been used to track recycling of exogenic sulfur into plume systems (Cabral et al., 2013; Delavault et al., 2016; Labidi et al., 2015), to identify an isotopic imprint of planetary differentiation (Labidi et al., 2013), and to trace magmatic processes such as degassing (Beaudry et al., 2018). The observation of mass-independent ($\Delta^{33}S \neq 0$) and mass-dependent ($\Delta^{33}S = 0$, variable $\delta^{34}S$) signatures of sulfur in mantle samples highlights its potential value for study in other mantle systems. The samples studied here yield a relationship between $\mu^{182}W$ and $^{3}He/^{4}He$ that illustrate a contribution from a primordial component (negative $\mu^{182}W$ anomalies associated with high $^{3}He/^{4}He$) and a non-primordial component. This offers an opportunity to place constraints on the primordial sulfur isotope composition of the mantle and to offer insight into the source of non-primordial W and He isotope compositions.

2. Geologic context/background

2.1. Samoan radiogenic isotopic geochemistry

Samoa is historically seen as sampling the archetypical Enriched Mantle-II (EMII) mantle source (e.g. Zindler and Hart, 1986). More recent work on radiogenic isotope signatures of lead (Pb) argues that the various Samoan volcanoes receive contributions from multiple mantle endmember sources (Jackson et al., 2014) including a depleted component, recycled components, and a primordial component, and these are sampled in the Vai, Malu, and Upo volcanic lineaments. Radiogenic isotopic compositions of strontium (Sr), neodymium (Nd), and lead (Pb) for samples from Samoa reveal signatures of recycled, subducted oceanic and continental crust in endmembers such as: the Enriched Mantle 1 (EMI) component in rejuvenated Samoan lavas, the Enriched Mantle 2 (EMII) component at Malumalu seamount and Savai'i submarine lavas, and the dilute HIMU (high $\mu = {}^{238}U/{}^{204}Pb$) component at Ta'u island and Vailulu'u seamount (Jackson et al., 2014; Workman et al., 2004). The EMI endmember is characterized by relatively low $^{143}Nd/^{144}Nd$ and $^{206}Pb/^{204}Pb$ at high $^{87}Sr/^{86}Sr$, and high $^{208}Pb/^{204}Pb$ at a given $^{206}Pb/^{204}Pb$. The EMII source is characterized by the highest $^{87}Sr/^{86}Sr$ and $^{208}Pb/^{204}Pb$ at a given $^{206}Pb/^{204}Pb$ and its origin is argued to reflect the subduction and recycling of continental sediments (Jackson et al., 2007a; Workman et al., 2008). The HIMU endmember is thought to reflect recycled oceanic crust after it experienced Pb loss during subduction, hence leading to ingrowth of radiogenic $^{206}Pb/^{204}Pb$ (e.g. Kelley et al., 2005 and references within).

Studies of ocean island basalts, including Samoa, also suggest various ocean islands host primordial mantle components. Evidence for this comes from high $^{3}He/^{4}He$ ratios in Hawaii (e.g. Kurz et al., 1983; Valbracht et al., 1997 and references within), Samoa (Jackson et al., 2009; 2007b), Iceland (e.g. Macpherson et al., 2005 and references within), Galapagos (Graham et al., 1993; Kurz et al., 2009), and Baffin Island (Starkey et al., 2009; Stuart et al., 2003). Additional evidence for early-formed "primordial" mantle domains is observed through the association of primitive Ar and Ne, and ancient Xe isotope signatures in mantle plumes with high $^{3}He/^{4}He$ (e.g. Kurz et al., 2009; Mukhopadhyay, 2012), negative $\mu^{182}W$ compositions associated with high $^{3}He/^{4}He$ in Samoa and Hawaii (Mundl et al., 2017), and positive $\mu^{182}W$ in Baffin island and Ontong Java Plateau (Rizo et al., 2016; also see Kruijer and Kleine, 2018).

2.2. Unique seismic structures beneath Samoa

In addition to the isotopic heterogeneity observed in the mantle, seismic evidence for compositional heterogeneity in the deep mantle has been mounting. Recent studies confirm that at the largest scales, the pair of Large low Shear Velocity Province (LLSVPs) appear to be associated with both low shear wavespeed and high density, a telltale signature of compositional heterogeneity (Lau et al., 2017; Moulik and Ekström, 2016). At smaller scales, Ultra Low Velocity Zones (ULVZs), whose properties have been interpreted to represent either partial melt (Williams and Garnero, 1996) or very high iron enrichment (Wicks et al., 2010), have now been detected beneath Samoa (Thorne et al., 2013), Hawaii (Cot-

taar and Romanowicz, 2012), and Iceland (Yuan and Romanowicz, 2017). High resolution global tomographic models constructed using full waveform inversion have been interpreted to require the presence of compositional heterogeneity within plume conduits themselves (French and Romanowicz, 2015). Importantly, efforts in mantle geochemistry have begun to associate mantle reservoirs that host primordial components, such as that sampled by Samoa, to Large Low shear Velocity Provinces (e.g. Williams et al., 2019) and Ultra Low Velocity Zones (e.g. Mundl et al., 2017) that reside at the base of the mantle. These observations continue to contribute evidence that mantle plumes are sampling reservoirs that are both deep and compositionally distinct from the ambient mantle.

3. Methods

Splits (1 to 3 gram aliquots) of the same fine crushed powder from Mundl et al. (2017) were placed into Teflon reactors for acid digestion as described by Labidi et al. (2012). These samples are a different type from those studied by Labidi et al. (2015) in that the samples are not glasses but, are rather the same powder from the interiors of the sampled flows used by Mundl et al. (2017). Prior to digestion, the setup was degassed with N_2 for $\sim$ 15 min. After degassing, the samples were acidified and digested in heated (70-80 °C) 3.2M $CrCl_2$, 12M HCl, and 29M HF in the amounts of 10 ml, 5 ml, and 5 ml respectively. The amount of solution was doubled for larger samples (>2 grams of powder). Sulfides were released as H_2S that is then bubbled (pulsed bubbling of ~3-5 bubbles every ~1-2 s) through a water trap and lastly trapped as Ag_2S in an acidic $AgNO_3$ trap solution. The captured Ag_2S subsequently transferred to a 1.5 ml Eppendorf centrifuge tube where it was then rinsed, agitated with a vortex machine for 10 s, and centrifuged with Milli-Q water. The supernatant was pipetted off and the rinsing procedure was repeated 6 times. After rinsing, the Ag_2S was dried at 70 °C. The dried Ag_2S was then weighed to determine sulfur concentration and the Ag_2S (0.3 mg to 5 mg) reacted with 3-5 times excess F_2 in heated (~250 °C) nickel reaction tubes for at least 8 h. Note, some samples yielded greater than 5 mg of Ag_2S (up to 15 mg). For these samples, 3-5 mg splits were taken and used for isotopic analyses. The resulting SF_6 was transferred to a liquid nitrogen cooled trap and the residual F_2 was passivated by a reaction with ~110 °C KBr salt. After passivation, the liquid nitrogen trap was replaced by an ethanol slush (~−108 °C to −115 °C) in an effort to separate HF from the remaining SF_6. Once separated, the SF_6 was transferred to a liquid nitrogen cooled injection loop of a gas chromatograph (GC). Next, the SF_6 was simultaneously thawed and injected into the gas chromatograph with flowing helium at a rate of 20 mL/min. The gas chromatograph allows for a final SF_6 purification using a 1/8-inch diameter, 20-foot long Haysep-Q™ GC column. The SF_6 was monitored while passing through the (GC) and captured from the helium flow in liquid nitrogen cooled spiral metal tubes. Lastly, the captured purified SF_6 was measured manometrically to determine procedural yields and preserved in individual sample fingers of glass manifolds. Yields determined from fluorination range from 70% to 106%. The glass manifold was then attached to an additional liquid nitrogen cooled manifold that is used to introduce SF_6 into the sample bellows of a Thermo Finnigan MAT 253 dual-inlet mass spectrometer.

3.1. Mass spectrometry

Sulfur has four stable isotopes (^{32}S (95.2%), ^{33}S (0.75%), ^{34}S (4.25%), and ^{36}S (0.02%)), and isotopic variations of sulfur isotopes were determined using mass spectrometry of purified SF_6. The purified SF_6 was measured by monitoring SF_5^+ ion beams at m/z of 127, 128, 129, and 131. Data are reported in per mil using the following notation:

$$\delta^{33}S = [((^{33}S/^{32}S)_{sample}/(^{33}S/^{32}S)_{CDT}) - 1]$$

$$\delta^{34}S = [((^{34}S/^{32}S)_{sample}/(^{34}S/^{32}S)_{CDT}) - 1]$$

$$\delta^{36}S = [((^{36}S/^{32}S)_{sample}/(^{36}S/^{32}S)_{CDT}) - 1]$$

$$\Delta^{33}S = [((^{33}S/^{32}S)_{sample}/(^{33}S/^{32}S)_{CDT}) - ((^{34}S/^{32}S)_{sample}/(^{34}S/^{32}S)_{CDT})^{0.515}]$$

$$\Delta^{36}S = [((^{36}S/^{32}S)_{sample}/(^{36}S/^{32}S)_{CDT}) - ((^{34}S/^{32}S)_{sample}/(^{34}S/^{32}S)_{CDT})^{1.9}]$$

All analyses were normalized to analyses of a large, single reservoir of SF_6 gas produced by fluorination of IAEA-S1 undertaken in the same session as the sample analyses. This normalization was conducted during each analytical session to account for changes in the composition of different aliquots of mass spectrometer reference gas. We developed this approach for studies of meteorite samples and found that the approach yields more accurate and reproducible $\Delta^{33}S$ (Antonelli et al., 2014). The data are then normalized to the value measured for Canyon Diablo Troilite (CDT) using the same approach and calibration in Antonelli et al. (2014) and Dottin et al. (2018). This places IAEA-S1 at a value of $\delta^{33}S = -0.091‰$, $\delta^{34}S = -0.401‰$, $\delta^{36}S = -1.558‰$, $\Delta^{33}S = 0.116‰$, $\Delta^{36}S = -0.796‰$.

Estimates of uncertainty can be assigned on the basis of measured long-term reproducibility of independent fluorinations of a variety of reference materials. These uncertainties include contributions from mass spectrometry and chemical preparation and, for $\Delta^{33}S$, vary depending on the mass spectrometry counting times. For $\delta^{34}S$ and $\Delta^{36}S$ the long-term reproducibility on reference materials is ±0.3‰ and ±0.3‰ (2σ). For $\Delta^{33}S$, the long-term reproducibility is ±0.008‰, and ±0.016‰ (2σ), for mass spectrometry analyses made using 9 and 3 analytical cycles, respectively.

The reproducibility reported in Table 1 of 2 (SE) represents the in-run precision from mass spectrometry and renormalization determined by Monte Carlo error propagation. The reproducibility (SE) for $\delta^{34}S$ and $\Delta^{36}S$ is smaller than seen from the long-term reproducibility on IAEA-S1 due to factors associated with the chemical procedures in preparing the SF_6 ($\delta^{34}S$) and interferences ($\Delta^{36}S$). The reproducibility (SE) is comparable to that seen for $\Delta^{33}S$ on the basis of long-term reproducibility on IAEA-S1. This suggests greatest contributor to reproducibility for $\Delta^{33}S$ comes from mass spectrometry. Estimates of precision (total uncertainty) are assumed to be the larger of the long-term reproducibility of reference materials and the propagated, normalized mass spectrometry data. These are presented in Table 1. For figures we plot estimated uncertainty. We use a Bayesian approach (details given in supplementary information) to assess match between data and models for relationships between sulfur isotope data and other geochemical systems.

4. Results

Data from 7 Samoan basalts are presented in Table 1 and Fig. 2. Sulfur concentrations of the bulk rock phase represent a lower limit, as a small amount of S could be lost in the sample preparation (rinsing and weighing procedure). Concentrations range from 30 ppm to 800 ppm S and isotopic compositions extend from +1.08 to +4.23‰ (± 0.3), −0.004 to +0.027‰ (± 0.008), and −0.29 to +0.22‰ (± 0.3) in $\delta^{34}S$, $\Delta^{33}S$, and $\Delta^{36}S$ respectively. With the exception of sample Ofu-04-15 ($\delta^{34}S = +4.23‰$), the $\delta^{34}S$ data are within the range of compositions previously reported (+0.11‰ to +2.79‰, Labidi et al., 2015). The $\Delta^{33}S$ and $\Delta^{36}S$ are all within the previously reported range, +0.001‰ to +0.022‰,

Table 1
Compilation of new S-isotope data and previously published radiogenic isotope data.

Location	Sample	Dredge depth (bars)	S (ppm)	$\delta^{34}S$ (‰)	†	‡	$\Delta^{33}S$ (‰)	†	‡	$\Delta^{36}S$ (‰)	†	‡	$\mu^{182}W$	2 SE		$^3He/^4He$ (R_A)			$^{206}Pb/^{204}Pb$		
Samoa																	2σ			2σ	
Vailulu'u	AVON3-63-2	92	809	1.23	0.028	0.3	0.019	0.010	0.016	−0.47	0.02	0.3	−4.9	2.1	a	10.06	0.1	c	19.3578	0.0018	c
	AVON3-70-9	113	201	2.30	0.015	0.3	0.027	0.012	0.016	−0.22	0.03	0.3	−5.8	5.2	a	8.05	0.2	d	19.3960	0.0004	c
	AVON3-71-22	417	603	2.09	0.005	0.3	0.009	0.006	0.008	0.08	0.03	0.3	−2.8	4	a	9.64	0.2	d	19.358	0.0194	d
	AVON3-73-1	96	214	1.88	0.003	0.3	0.01	0.004	0.008	−0.02	0.02	0.3	−7.7	3.8	a	8.1	0.2	d	19.2299	0.0002	c
Malumalu	AVON 3-77-1	361	393	1.97	0.007	0.3	0.004	0.006	0.008	−0.01	0.02	0.3	−7.45	4††	a	13.45	0.2	d	19.2683	0.0003	c
Ofu	OFU-04-15	0	64	4.23	0.009	0.3	0.001	0.004	0.008	0.22	0.06	0.3	−13.7	4.8 (2 S.D.)	e	29.6	0.4	b	19.1410	0.00190	b
	OFU-05-18**	0	29	1.08	0.015	0.3	−0.004	0.004	0.008	0.13	0.03	0.3	−13.8	3.3	a	33.7	0.4	b	19.1890	0.00190	b

† Reproducibility (2 Standard Error) determined using a Monte Carlo error propagation that takes into account the in-run precision on measurements of IAEA-S1 during the analytical session and the sample.
‡ Estimated uncertainty from long-term reproducibility on standard materials.
†† The error reported here and shown in Fig. 2 and 3 is the long-term external reproducibility reported in Mundl et al. (2017).
(a) (Mundl et al., 2017), (b) (Jackson et al., 2007a; 2007b), (c) (Jackson et al., 2014), (d) (Workman et al., 2004), (e) (Mundl-Petermeier et al., 2020). †† Average composition of two analyses of same sample by Mundl et al. (2017).
** Note that Ofu-05-18 is a resampling of the same dike as sample Ofu-04-06 in Jackson et al. (2007a; 2007b).

Fig. 2. Compilation of new and existing S-isotope data ($\delta^{34}S$ vs. $\Delta^{33}S$) for various OIB and MORB sources. New data plotted are from bulk rock powders (blue and red symbols) from the Vailulu'u, Malumalu, and Ofu volcanoes of Samoa. The remaining data is collected either as glass (Labidi et al., 2013; 2014; 2015) or as individual sulfides using Secondary Ion Mass Spectrometry (SIMS) (Cabral et al., 2013; Delavault et al., 2016. The data we report fall within the range of compositions reported on glasses by Labidi et al., 2015 with the exception of 1 data point from Ofu (Ofu-04-15). Note, the compositions shown from Labidi et al. (2013; 2014; 2015) are not shifted to the CDT scale in $\delta^{34}S$ and the UMD-CDT scale for $\Delta^{33}S$. This shift in normalization yields a −0.1 ‰ shift in $\delta^{34}S$ and a +0.01 ‰ shift in $\Delta^{33}S$. The error bars on $\delta^{34}S$ are an estimate from the long-term reproducibility on standards that takes into account the uncertainty associated with sample processing. Error bars on $\Delta^{33}S$ represent estimates from the long-term reproducibility on standard materials (see methods). (For interpretation of the colors in the figure(s), the reader is referred to the web version of this article.)

and −0.063‰ to +0.271‰, for $\Delta^{33}S$ and $\Delta^{36}S$ respectively.[1] The compositions we observe are within the range of bulk sulfur isotope compositions reported for the global dataset of glasses from ocean island and mid ocean ridge basalts where values range from ∼ −3‰ to +3‰ in $\delta^{34}S$ and −0.01‰ to +0.01‰ in $\Delta^{33}S$ (Labidi et al., 2015; 2014; 2013). However, the observed compositions are not as extreme as the isotopic data obtained on individual sulfides via secondary ion mass spectrometry (SIMS), at localities such as the Canary Islands that reveal large negative $\delta^{34}S$ variations (up to −8.2‰) assigned to degassing with strictly mass dependent $\Delta^{33}S$ (Beaudry et al., 2018) and Mangaia and Pitcairn that show large negative $\delta^{34}S$ variations (−17.25‰ to −2.25‰) associated with sub-permil $\Delta^{33}S$ variations (0 to −0.85 ‰) (Cabral et al., 2013; Delavault et al., 2016). These SIMS measurements resolve isotopic difference on a granular scale, which is different from bulk measurements presented here, and have larger uncertainties.

Our data reveal relationships between $\Delta^{33}S$ and radiogenic isotopic compositions of W, Pb, and He. The data do not, however,

[1] The compositions reported here are not shifted to the CDT scale in $\delta^{34}S$ and the UMD-CDT scale for $\Delta^{33}S$. This shift in normalization yields a −0.1‰ shift in $\delta^{34}S$ and a +0.01‰ shift in $\Delta^{33}S$ which would convert to +0.01 to +2.69, +0.011 to +0.032, and −0.063 to +0.271 for in $\delta^{34}S$, $\Delta^{33}S$, and $\Delta^{36}S$ respectively.

preserve a relationship between $\delta^{34}S$ and radiogenic isotopic compositions of W, Pb, and He. In order to assess the significance of these relationships, we employed a Bayesian model selection approach to quantify the relative probability that the underlying relationship is represented by a line (M1) versus a constant value (i.e. line with zero slope; M2). We explicitly marginalize out the extra tunable parameter (slope of the line) present in M1, and assume that the errors in both composition estimates are normally distributed and uncorrelated. We find that the radiogenic W, Pb, and He vs. $\Delta^{33}S$ data strongly prefer M1 over M2 (>99% chance of being true).

5. Discussion

5.1. Preservation of mantle sulfur in interiors of pillow basalts?

We report sulfur concentrations in the interior of pillow basalts erupted at Ofu, Vailulu'u and Malumalu that range from 30 to 800 ppm. These are lower than concentrations seen in glasses erupted at these islands (600 to 2000 ppm S, Labidi et al., 2015). Typically, samples of glass, erupted at ocean depths greater than 1000 meters have the greatest chance of preserving the sulfur concentrations and isotopic compositions of the erupted melt (Moore and Fabbi, 1971). The bulk rock samples from Vailulu'u and Malumalu are from submarine eruptions (they were collected at water depths of ≥92 bars) and preserve slightly higher sulfur concentrations, but are at the low end (600-800 ppm) of the S concentrations reported for samples of glass from the same localities by Workman et al. (2006) and Labidi et al. (2015) and in some cases (see Table 1, supplementary figure 2) reveal even lower concentrations (∼200 ppm) than the lowest value (∼600 ppm) reported by Labidi et al. (2015). Bulk rock samples with the lowest S concentrations (30 and 60 ppm S) are subaerial lavas from Ofu. Sulfur loss can also be associated with isotopic shifts in $\delta^{34}S$, but not $\Delta^{33}S$ or $\Delta^{36}S$.

The sulfur isotope compositions of Samoan basalts (from this study and Labidi et al., 2015) are ^{34}S-enriched relative to the composition of mantle sulfur proposed by Labidi et al. (2013; 2014) of $-1\pm0.5‰$. These ^{34}S-enrichments could be caused by recycling of ^{34}S-bearing subducted components (Labidi et al., 2015), or by syn-eruptive or post-eruptive sulfur loss. While sulfur loss could be accounted for by episodes of sulfide segregation, as seen in some Samoan melts (Labidi et al., 2015), we argue that the lowest sulfur concentrations observed here illustrate sulfur loss through an event(s) of sulfur degassing and that the loss of sulfur (^{32}S) could account for the increasing ^{34}S-enriched characteristic of the Ofu samples ($\delta^{34}S = +1.8‰$ and $+4.3‰$). A similar shift in $\delta^{34}S$ from degassing cannot be ruled out for the samples from Vailulu'u and Malumalu, however, some of these samples still overlap the range of sulfur isotopic compositions seen for Samoan glasses by Labidi et al. (2015) (Fig. 2).

Sulfur loss through degassing can occur as an equilibrium fractionation, a kinetic fractionation, or a combination of both. At the Quartz-Fayalite-Magnetite reaction buffer, SO_2 dominates the gas phase (Burgisser et al., 2015; Gaillard and Scaillet, 2009), and degassing is expected for melts erupting at less than 100 bars pressure (∼1000 m depth) (Gaillard and Scaillet, 2009). At 1200 °C, sulfur dioxide is ^{34}S-enriched by ∼1.5 to 3‰ relative to the dissolved sulfide in the melt (e.g. Mandeville et al., 2009), and equilibrium degassing of sulfur dioxide drives the melt to more negative $\delta^{34}S$ compositions. If instead the S were degassed as H_2S, S loss would result in a negligible fractionation of ^{34}S (Mandeville et al., 2009) but H_2S loss is not supported by degassing models of melts with these compositions and oxygen fugacities (Burgisser et al., 2015). The alternative, kinetic degassing, results upon rapid loss of S and generates a ^{34}S heavy residual melt, rather than depletion, driving the melt towards positive $\delta^{34}S$ (e.g. de Moor et al., 2013 and references within). Note, positive $\delta^{34}S$ can be achieved during decompression degassing in highly oxidizing conditions (>QFM +3, Fiege et al., 2014). Degassing almost certainly occurred, however our data do not allow for a single process with a singular fractionation to be identified (supplementary figure 1). This limits our ability to project back to the $\delta^{34}S$ of an initial magma. We note that oxidative weathering of the crystalline interiors may have induced the loss of reduced S. Studies of isotope effects associated with low temperature oxidation by Heidel et al. (2013) show no change in the $\delta^{34}S$ of the residual sulfides from oxidation, but, reveal a fractionation for the product sulfate which they attribute to formation of more than one product. Thus, in the event of oxidative weathering, it is expected that the $\delta^{34}S$ of sulfide would still reflect that of its parental melt.

5.2. Recycled sulfur in Samoa

The submarine erupted samples we analyzed from Vailulu'u and Malumalu have higher S concentrations than the analyzed Ofu samples and we suggest (see above) that sulfur degassing may have only minimally modified the isotopic composition. These samples have $\delta^{34}S$ compositions (+1.23 to +2.30‰) that fall within the range of values previously reported on glassy Samoan basalts by Labidi et al. (2015) and exhibit similar radiogenic isotope compositions for Pb, Sr, and He (Fig. 3). Even though the sulfur concentrations are generally lower than that observed by Labidi et al. (2015) (supplementary figure 2), the geochemical similarity between the samples suggests they are part of the same population. Thus, we defer to the study by Labidi et al. (2015) for insight into the $\delta^{34}S$ of the primary magma, where they identified a mixing array between a lower $^{87}Sr/^{86}Sr$ mantle domain with negative $\delta^{34}S$, and an EMII endmember with positive $\delta^{34}S$.

The relationship between $\Delta^{33}S$ and other geochemical systems such as tungsten, helium and lead isotopes reflects mixing of mantle reservoirs sampled by the Samoa mantle plume, including a recycled component with dilute HIMU characteristics (Jackson et al., 2014), an EMII sulfur component that has been documented by Labidi et al. (2015) and a primordial endmember defined by negative $\mu^{182}W$ and high $^{3}He/^{4}He$ (Mundl et al., 2017). Below, we explore in greater detail various scenarios for interpreting the relationships between sulfur and other geochemical systems. We start by discussing the connection with the recycled component and then discuss the connection with the primordial endmember in the context of its suggested origin and placement this endmember.

Our data from Vailulu'u and Malumalu occupy the same field for $\delta^{34}S$ and $^{87}Sr/^{86}Sr$ (Fig. 4) and also the same field for $\delta^{34}S$ vs $\Delta^{33}S$ (Fig. 2) as defined for volcanic glasses of the Samoan volcanic chain reported by Labidi et al. (2015). Labidi et al. (2015) argue that these relationships between $\delta^{34}S$ and $^{87}Sr/^{86}Sr$ reflect mixing between an EMII mantle endmember with positive $\delta^{34}S$ ($+10 \pm 3‰$) and radiogenic $^{87}Sr/^{86}Sr$ and a mantle domain with negative $\delta^{34}S_{V\text{-}CDT}$ (-0.89 ± 0.11 (1σ)) and less radiogenic $^{87}Sr/^{86}Sr$. Minor scatter in the $\Delta^{33}S$ of the combined data allows for other components with different $\Delta^{33}S$, such as HIMU, as underplating of HIMU-enriched material to the crust below Samoa has been proposed as the outcome of the earlier passage of the Cook-Austral plumes (Workman et al., 2004); however, the HIMU component may also be indigenous to the Samoan plume (Jackson et al., 2014). Jackson et al. (2014) argue that the Vailulu'u lavas reveal characteristics suggestive of a dilute HIMU signature. The slightly elevated $\Delta^{33}S$ in Vailulu'u lavas is interpreted to reflect a dilute contribution from a HIMU component that possess variable anomalous $\Delta^{33}S$. A similar observation is observed in lavas from Vailulu'u in Labidi et al. (2015). Given the data from Malumalu (EM2) and Vailulu'u (dilute HIMU) occupy different fields for $\delta^{34}S$ and $^{87}Sr/^{86}Sr$ and a slightly

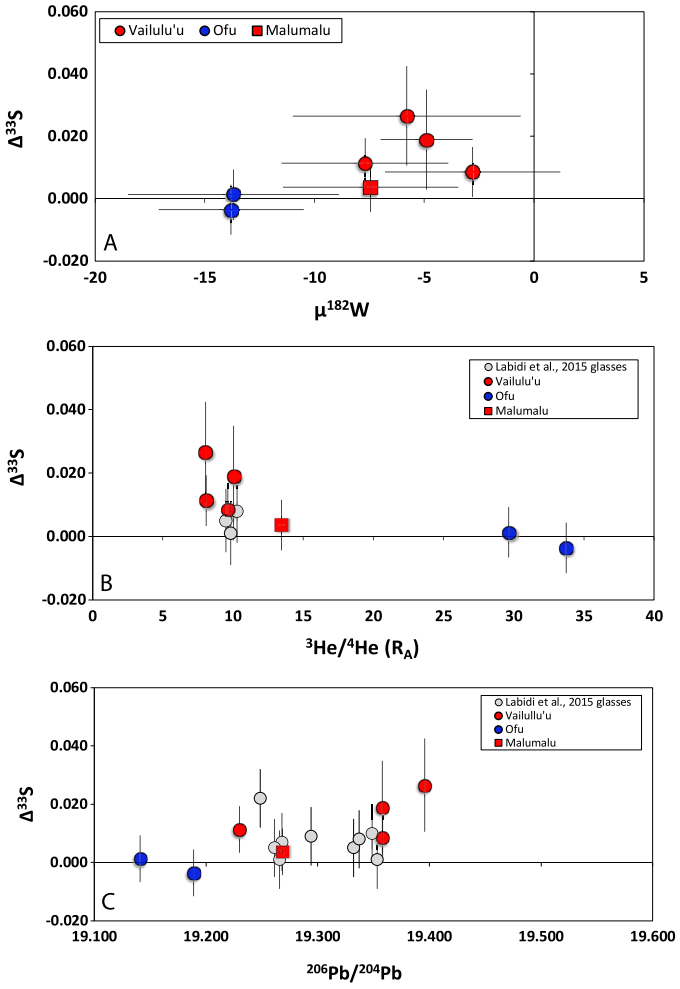

Fig. 3. This figure illustrates a relationship in (A) μ^{182}W vs. Δ^{33}S, (B) ^{3}He/^{4}He vs. Δ^{33}S, and (C) ^{206}Pb/^{204}Pb vs. Δ^{33}S. μ^{182}W data are from Mundl et al. (2017) and Mundl-Petermeier et al. (2020). ^{3}He/^{4}He data are from Jackson et al. (2007a) and Jackson et al. (2014). ^{206}Pb/^{204}Pb are from Jackson et al. (2007a, 2007b), Jackson et al. (2014), and Workman et al. (2004). Error for ^{3}He/^{4}He and ^{206}Pb/^{204}Pb are reported in Table 1 and are within the plotted symbols.

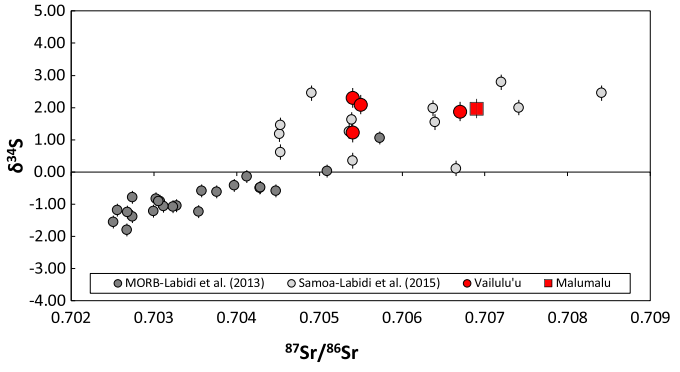

Fig. 4. Plot of ^{87}Sr/^{86}Sr versus δ^{34}S for data presented in this study (red, we exclude data from Ofu because these samples are from subaerial eruptions and likely reflect compositions affected by degassing) and data reported by (Labidi et al., 2015; 2013) (light and dark grey). Note, Labidi et al., 2015 propose the increasing δ^{34}S and ^{87}Sr/^{86}Sr relationship is the result of mixing with S-enriched upper continental crust with the conditions of either S/Sr = 50, δ^{34}S = +5‰ or S/Sr = 17, δ^{34}S = +10‰.

different field for δ^{34}S vs Δ^{33}S (Fig. 2), the case may be that the sources of sulfur are indeed different for the Vai and Malu volcanic lineament. The high ^{87}Sr/^{86}Sr in EM2 Malumalu lavas (and possibly the Vailulu'u lavas, which also have moderately elevated ^{87}Sr/^{86}Sr), combined with observed δ^{34}S vs Δ^{33}S, allows for a potential mixture of both Proterozoic and Archean sediments (Labidi et al., 2015). In this type of mixture, the small magnitude Δ^{33}S signature could also be contributed by Proterozoic sediments (See Johnston (2011) for data compilations showing such characteristics for early to middle Proterozoic sediments). Such small-magnitude positive and negative shifts of Δ^{33}S are a natural outcome of biological and biogeochemical cycling (Ono et al., 2006) and are seen in sulfide and sulfate from a wide range of sedimentary and hydrothermal systems (Johnston, 2011).

5.3. Sulfur from the primordial mantle

The plume component with which this recycled endmember is mixed hosts a heterogeneous radiogenic Pb isotopic composition. The data from Samoa define four arrays in ^{206}Pb/^{204}Pb vs. ^{204}Pb/^{204}Pb that all converge on a small range of values (19.0-19.3 in ^{206}Pb/^{204}Pb, 39.0-39.4 in ^{208}Pb/^{204}Pb) (Jackson et al., 2014) that are associated with the high ^{3}He/^{4}He ratios of the "common component" (20-33.8 R_A). Samples from Samoa with high ^{3}He/^{4}He also preserve negative μ^{182}W compositions (Mundl et al., 2017). Such ^{182}W deficits require a separate evolution from mantle-hosted ^{182}Hf, which went extinct within the first 60 million years of solar system history. ^{182}W deficits are thus signatures formed early in Earth's accretionary history that were immediately isolated from mantle convection and mixing (Mundl et al., 2017).

The observed relationships between S with He and W (Fig. 3) suggests the contribution of sulfur from an undegassed, early-formed mantle reservoir. Our data establish that materials linked to the deep primordial component have $\Delta^{33}S \approx 0$‰, similar to the average MORB value of 0.008 ± 0.006‰ ($n = 80$, 1 s.d., Labidi and Cartigny, 2016). A homogeneous mantle Δ^{33}S with variable μ^{182}W supports a process that homogenized Δ^{33}S prior to the ingrowth of μ^{182}W signatures in different reservoirs. In Samoan lavas, the recycled components bring materials with $\Delta^{33}S \neq 0$‰ associated with the recycled component with HIMU characteristics (Jackson et al., 2014) and the observed relationship is apparent because this component has a different Δ^{33}S than the endmember with negative μ^{182}W. It was shown that the convective mantle is defined by Δ^{33}S and μ^{182}W both equal to zero (e.g. Labidi et al., 2014; Willbold et al., 2011). We therefore expect future analyses will fill in a three-component mixing field for Δ^{33}S and μ^{182}W (though, hints of this field may already be present in Fig. 5); endmember 1 is a primordial component, endmember 2 is a recycled component, endmember 3 is the convecting mantle.

To allow for an early segregated metal-rich reservoir with a ^{182}W deficit, Mundl et al. (2017) suggest a connection to deep mantle reservoirs such as the seismically-defined Large Low Shear Velocity Province (LLSVP) or Ultra Low Velocity Zone (ULVZ) beneath Samoa which have been suggested to host Fe-rich metals (e.g. Zhang et al., 2016) and/or may have interacted with the core (Rizo et al., 2019). Work by Frost et al. (2004) suggests the formation of such metal could have occurred via an Fe^{2+} disproportionation pathway driven by formation of bridgmanite early in Earth's history. This process has the potential to yield a reservoir of deep mantle metal with moderate W abundances and low HSEs (Mundl et al., 2017). Zhang et al. (2016) point out that S will concentrate in this metal phase, which in turn will mute the expression of the equilibrium metal/silicate fractionation (>1‰: Labidi et al., 2016) and yield an isotopic composition similar to that of the mantle in which it formed (negative δ^{34}S and $\Delta^{33}S = 0$‰). This composition is consistent with the composition of sulfur we infer for the endmember with negative μ^{182}W.

An alternative proposed mechanism for producing negative μ^{182}W variations involve high-pressure episodes of core formation

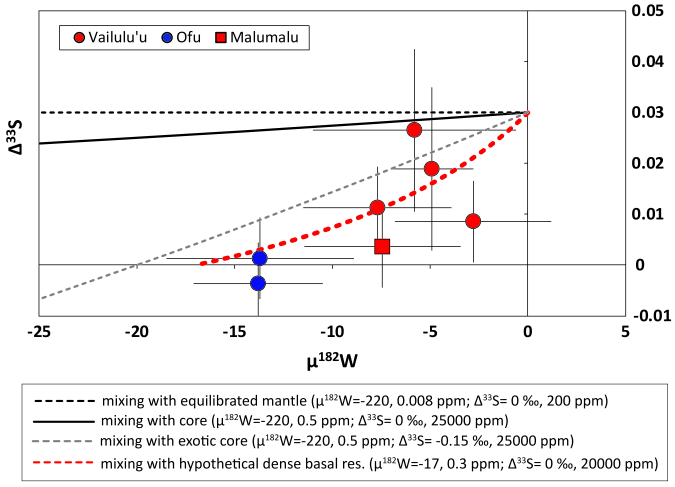

Fig. 5. Plot of μ^{182}W vs. Δ^{33}S illustrating scenarios for mixing of sulfur and tungsten between a primordial reservoir and a recycled component. Compositions for the primordial reservoir are denoted in parenthesis. We assign the recycled mantle endmember composition for all scenarios to be $\mu^{182}\text{W} = 0$, 0.008 ppm; $\Delta^{33}\text{S} = 0.03$, 200 ppm. This composition is chosen to illustrate how various models evolve from a composition matching the most ^{33}S-enriched sample in our data set.

that are recorded and preserved in the deep mantle (Jackson et al., 2018). At high pressure, sulfur remains a siderophile element (Suer et al. 2017) but the isotopic effect remains unconstrained. There is a potential for changes in the mass dependent fractionation of $^{34}\text{S}/^{32}\text{S}$ (see discussion in Labidi et al., 2016), but we consider it unlikely that the Δ^{33}S would be affected in the formation of the deep mantle reservoir.

Mundl et al. (2017) discount the possibility that physical core metal entrainment was the source of primordial (negative) μ^{182}W because HSEs are not sufficiently enriched in Samoan lavas and are uncorrelated with negative μ^{182}W. In consideration of the mantle nature of sulfur in samples with increasingly negative μ^{182}W from Vailulu'u and Malumalu,[2] the data suggest the primordial component likely has negative δ^{34}S, which would be inconsistent with the core being the source of the sulfur that was later diluted with recycled sediments. Labidi et al. (2013) and Labidi and Cartigny (2016) argue that the δ^{34}S of the bulk Earth, if chondritic, must be between -0.27 and $+0.04$‰. In this case, the mantle and core bracket this value with the mantle having strongly negative δ^{34}S (-0.89 ± 0.11‰ (1σ)) while the core is slightly ^{34}S-enriched. Further support for the Mundl et al. (2017) suggestion that the μ^{182}W anomalies did not originate from entrainment of core material, may be provided by the lack of significant curvature in the $\Delta^{33}\text{S} - \mu^{182}\text{W}$ array (Fig. 5) and the prevalence of near zero or slightly positive Δ^{33}S for early solar system materials (Antonelli et al., 2014). Significant curvature would be expected if the mantle mixed with core material to generate the $\Delta^{33}\text{S} - \mu^{182}\text{W}$ array (Fig. 5) observed here, due to different W/S ratios in the mantle and core. The lack of curvature also implies the W/S concentration ratio is not much different in the mixing endmembers and, unless the primordial reservoir has negative Δ^{33}S, the negative μ^{182}W endmember may not be significantly more negative (e.g. if it was a direct core contribution) than the most negative values that have been measured thus far.

More recent work by Mundl-Petermeier et al. (2020) introduce an argument for anomalous μ^{182}W that involves a chemical and isotopic equilibration process for W between a basal silicate layer and the core. Mundl-Petermeier et al. (2020) argue that the best candidate reservoirs are seismically imaged ULVZs. An equilibration process that generates a reservoir with μ^{182}W of ~-17 for a Δ^{33}S ~0 would explain our data (Mundl-Petermeier et al., 2020). The resulting reservoir would mix with a recycled endmember with $\Delta^{33}\text{S} \neq 0$ to produce the arrays that are seen. Using simple mixing calculations, the data are well fit with this model assuming the amount of tungsten mixed into the basal silicate reservoir yields a $\mu^{182}\text{W}$ of ~ -17.

6. Conclusions

The Samoan islands are the type locality for the EM (II) reservoir but also receive dilute contributions from EM (I), HIMU, and DMM related components. Furthermore, Samoa sits above a seismically imaged LLSVP and ULVZ that is thought to be the source of material that exhibit primordial isotope compositions, seen as high ^{3}He/^{4}He and negative μ^{182}W. We have characterized the nature of sulfur in primordial and recycled mantle sources using multiple sulfur isotopes of bulk rock Samoan basalts by focusing on Samoan islands with high ^{3}He/^{4}He and negative μ^{182}W. Relationships between Δ^{33}S and other geochemical systems such as radiogenic tungsten, helium and lead isotopes is observed and suggests mixing between a component with HIMU characteristics (slight positive Δ^{33}S and positive δ^{34}S) with a primordial endmember (negative μ^{182}W, high ^{3}He/^{4}He, $\Delta^{33}\text{S} = 0$ and negative δ^{34}S). The antiquity of the primordial endmember is indicated by ^{182}W deficits that require a separate evolution from mantle-hosted ^{182}Hf within the first 60 million years of solar system history. The similar indistinguishable Δ^{33}S from that of the convective mantle indicates that sulfur isotopes were thus homogenized early in Earth's history. The small but resolvable Δ^{33}S in the recycled endmember reflects sulfur that is contributed by a Samoan plume component with HIMU characteristics (with a possible mixture of Proterozoic sulfur from continental crust sediments). Although a contribution from mass-independent Archean Δ^{33}S could be associated with HIMU, it is not required to explain the Δ^{33}S variation because younger (Proterozoic) contributions may also have small positive and negative deviations from $\Delta^{33}\text{S} = 0$. The correlations between sulfur, Pb, He, and W are most easily reconciled with a deep mantle process linked to a dense, undegassed basal reservoir such as a ULVZ. Although our data do not support a reservoir with $\mu^{182}\text{W} = -220$ and $\Delta^{33}\text{S} = 0$, the relationship between sulfur and tungsten could reflect W isotope equilibration through a core-mantle equilibration process, where a diluted core W isotope composition having less negative μ^{182}W is incorporated into the plume that also hosts recycled sediments having $\Delta^{33}\text{S} \neq 0$. Ultimately, our work identifies relationships between sulfur and radiogenic Pb, He, and W that provide a means of continuing to unravel the complexities of geochemical heterogeneity of the mantle. With this work, we further the understanding of how the subduction and recycling of oceanic and continental crust can influence geochemical signatures observed at ocean islands and how well dispersed the various reservoirs are in the mantle.

Declaration of competing interest

The authors declare that they have no known competing financial interests or personal relationships that could have appeared to influence the work reported in this paper.

Acknowledgements

We sincerely thank Editor Tamsin Mather for handling our manuscript and providing useful comments. We also appreciate the

[2] We set aside the data for two samples from Ofu because of the likelihood of late shifts of δ^{34}S from extreme degassing owing to shallow eruption of the Ofu lavas.

thoughtful comments and suggestions from three anonymous reviewers. This project was supported by the University of Maryland Graduate School Research and Scholarship Award and a Fulbright Fellowship (JF). The manuscript was partially constructed while JF was visiting at the Institut de Physique du Globe Paris (IPGP).

Appendix A. Supplementary material

Supplementary material related to this article can be found online at https://doi.org/10.1016/j.epsl.2020.116073.

References

Antonelli, M.A., Kim, S.-T., Peters, M., Labidi, J., Cartigny, P., Walker, R.J., Lyons, J.R., Hoek, J., Farquhar, J., 2014. Early inner solar system origin for anomalous sulfur isotopes in differentiated protoplanets. Proc. Natl. Acad. Sci. USA 111, 17749–17754. https://doi.org/10.1073/pnas.1418907111.

Beaudry, P., Longpré, M.-A., Economos, R., Wing, B.A., Bui, T.H., Stix, J., 2018. Degassing-induced fractionation of multiple sulphur isotopes unveils post-Archaean recycled oceanic crust signal in hotspot lava. Nat. Commun. 9, 5093.

Burgisser, A., Alletti, M., Scaillet, B., 2015. Simulating the behavior of volatiles belonging to the C–O–H–S system in silicate melts under magmatic conditions with the software D-Compress. Comput. Geosci. 79, 1–14.

Cabral, R.A., Jackson, M.G., Rose-Koga, E.F., Koga, K.T., Whitehouse, M.J., Antonelli, M.A., Farquhar, J., Day, J.M.D., Hauri, E.H., 2013. Anomalous sulphur isotopes in plume lavas reveal deep mantle storage of Archaean crust. Nature 496, 490–493. https://doi.org/10.1038/nature12020.

Cottaar, S., Romanowicz, B., 2012. An unusually large ULVZ at the base of the mantle near Hawaii. Earth Planet. Sci. Lett. 355, 213–222.

de Moor, J.M., Fischer, T.P., Sharp, Z.D., King, P.L., Wilke, M., Botcharnikov, R.E., Cottrell, E., Zelenski, M., Marty, B., Klimm, K., 2013. Sulfur degassing at Erta Ale (Ethiopia) and Masaya (Nicaragua) volcanoes: implications for degassing processes and oxygen fugacities of basaltic systems. Geochem. Geophys. Geosyst. 14, 4076–4108.

Delavault, H., Chauvel, C., Thomassot, E., Devey, C.W., Dazas, B., 2016. Sulfur and lead isotopic evidence of relic Archean sediments in the Pitcairn mantle plume. Proc. Natl. Acad. Sci. 113, 12952–12956. https://doi.org/10.1073/pnas.1523805113.

Dottin, J.W., Farquhar, J., Labidi, J., 2018. Multiple sulfur isotopic composition of main group pallasites support genetic links to IIIAB iron meteorites. Geochim. Cosmochim. Acta 224, 276–281. https://doi.org/10.1016/j.gca.2018.01.013.

Fiege, A., Holtz, F., Shimizu, N., Mandeville, C.W., Behrens, H., Knipping, J.L., 2014. Sulfur isotope fractionation between fluid and andesitic melt: an experimental study. Geochim. Cosmochim. Acta 142, 501–521.

French, S.W., Romanowicz, B., 2015. Broad plumes rooted at the base of the Earth's mantle beneath major hotspots. Nature 525, 95.

Frost, D.J., Liebske, C., Langenhorst, F., McCammon, C.A., Trønnes, R.G., Rubie, D.C., 2004. Experimental evidence for the existence of iron-rich metal in the Earth's lower mantle. Nature 428, 409.

Gaillard, F., Scaillet, B., 2009. The sulfur content of volcanic gases on Mars. Earth Planet. Sci. Lett. 279, 34–43.

Graham, D.W., Christie, D.M., Harpp, K.S., Lupton, J.E., 1993. Mantle plume helium in submarine basalts from the Galápagos platform. Science 80 (262), 2023–2026.

Heidel, C., Tichomirowa, M., Junghans, M., 2013. Oxygen and sulfur isotope investigations of the oxidation of sulfide mixtures containing pyrite, galena, and sphalerite. Chem. Geol. 342, 29–43.

Jackson, C.R.M., Bennett, N.R., Du, Z., Cottrell, E., Fei, Y., 2018. Early episodes of high-pressure core formation preserved in plume mantle. Nature 553, 491–495. https://doi.org/10.1038/nature25446.

Jackson, M.G., Hart, S.R., Koppers, A.A.P., Staudigel, H., Konter, J., Blusztajn, J., Kurz, M., Russell, J.A., 2007a. The return of subducted continental crust in Samoan lavas. Nature 448, 684.

Jackson, M.G., Kurz, M.D., Hart, S.R., Workman, R.K., 2007b. New Samoan lavas from Ofu Island reveal a hemispherically 264, 360–374. https://doi.org/10.1016/j.epsl.2007.09.023.

Jackson, M.G., Kurz, M.D., Hart, S.R., 2009. Helium and neon isotopes in phenocrysts from Samoan lavas: evidence for heterogeneity in the terrestrial high 3He/4He mantle. Earth Planet. Sci. Lett. 287, 519–528. https://doi.org/10.1016/j.epsl.2009.08.039.

Jackson, M.G., Hart, S.R., Konter, J.G., Kurz, M.D., Blusztajn, J., Farley, K.A., 2014. Helium and lead isotopes reveal the geochemical geometry of the Samoan plume. Nature 514, 355–358. https://doi.org/10.1038/nature13794.

Johnston, D.T., 2011. Multiple sulfur isotopes and the evolution of Earth's surface sulfur cycle. Earth-Sci. Rev. 106, 161–183. https://doi.org/10.1016/j.earscirev.2011.02.003.

Kelley, K.A., Plank, T., Farr, L., Ludden, J., Staudigel, H., 2005. Subduction cycling of U, Th, and Pb. Earth Planet. Sci. Lett. 234, 369–383.

Kruijer, T.S., Kleine, T., 2018. No 182W excess in the Ontong Java Plateau source. Chem. Geol. 485, 24–31.

Kurz, M.D., Jenkins, W.J., Hart, S.R., Clague, D., 1983. Helium isotopic variations in volcanic rocks from Loihi Seamount and the Island of Hawaii. Earth Planet. Sci. Lett. 66, 388–406. https://doi.org/10.1016/0012-821X(83)90154-1.

Kurz, M.D., Curtice, J., Fornari, D., Geist, D., Moreira, M., 2009. Primitive neon from the center of the Galápagos hotspot. Earth Planet. Sci. Lett. 286, 23–34.

Labidi, J., Cartigny, P., 2016. Negligible sulfur isotope fractionation during partial melting: evidence from Garrett transform fault basalts, implications for the late-veneer and the hadean matte. Earth Planet. Sci. Lett. 451, 196–207.

Labidi, J., Cartigny, P., Birck, J.L., Assayag, N., Bourrand, J.J., 2012. Determination of multiple sulfur isotopes in glasses: a reappraisal of the MORB δ^{34}S. Chem. Geol. 334, 189–198.

Labidi, J., Cartigny, P., Moreira, M., 2013. Non-chondritic sulphur isotope composition of the terrestrial mantle. Nature 501, 208–211. https://doi.org/10.1038/nature12490.

Labidi, J., Cartigny, P., Hamelin, C., Moreira, M., Dosso, L., 2014. Sulfur isotope budget (32S, 33S, 34S and 36S) in Pacific-Antarctic ridge basalts: a record of mantle source heterogeneity and hydrothermal sulfide assimilation. Geochim. Cosmochim. Acta 133, 47–67. https://doi.org/10.1016/j.gca.2014.02.023.

Labidi, J., Cartigny, P., Jackson, M.G., 2015. Multiple sulfur isotope composition of oxidized Samoan melts and the implications of a sulfur isotope 'mantle array' in chemical geodynamics. Earth Planet. Sci. Lett. 417, 28–39. https://doi.org/10.1016/j.epsl.2015.02.004.

Labidi, J., Shahar, A., Le Losq, C., Hillgren, V.J., Mysen, B.O., Farquhar, J., 2016. Experimentally determined sulfur isotope fractionation between metal and silicate and implications for planetary differentiation. Geochim. Cosmochim. Acta 175, 181–194. https://doi.org/10.1016/j.gca.2015.12.001.

Lau, H.C.P., Mitrovica, J.X., Davis, J.L., Tromp, J., Yang, H.-Y., Al-Attar, D., 2017. Tidal tomography constrains Earth's deep-mantle buoyancy. Nature 551, 321.

Macpherson, C.G., Hilton, D.R., Day, J.M.D., Lowry, D., Grönvold, K., 2005. High-3He/4He, depleted mantle and low-δ18O, recycled oceanic lithosphere in the source of central Iceland magmatism. Earth Planet. Sci. Lett. 233, 411–427.

Mandeville, C.W., Webster, J.D., Tappen, C., Taylor, B.E., Timbal, A., Sasaki, A., Hauri, E., Bacon, C.R., 2009. Stable isotope and petrologic evidence for open-system degassing during the climactic and pre-climactic eruptions of Mt. Mazama, Crater Lake, Oregon. Geochim. Cosmochim. Acta 73, 2978–3012. https://doi.org/10.1016/j.gca.2009.01.019.

Moore, J.G., Fabbi, B.P., 1971. An estimate of the juvenile sulfur content of basalt. Contrib. Mineral. Petrol. 33, 118–127.

Moulik, P., Ekström, G., 2016. The relationships between large-scale variations in shear velocity, density, and compressional velocity in the Earth's mantle. J. Geophys. Res., Solid Earth 121, 2737–2771.

Mukhopadhyay, S., 2012. Early differentiation and volatile accretion recorded in deep-mantle neon and xenon. Nature 486, 101.

Mundl, A., Touboul, M., Jackson, M.G., Day, J.M.D., Kurz, M.D., Lekic, V., Helz, R.T., Walker, R.J., 2017. Tungsten-182 heterogeneity in modern ocean island basalts. Science 80 (356), 66–69. https://doi.org/10.1126/science.aal4179.

Mundl-Petermeier, A., Walker, R.J., Jackson, M.G., Blichert-Toft, J., Kurz, M.D., Halldórsson, S.A., 2019. Temporal evolution of primordial tungsten-182 and 3He/4He signatures in the Iceland mantle plume. Chem. Geol. 525, 245–259.

Mundl-Petermeier, A., Walker, R.J., Fischer, R.A., Lekic, V., Jackson, M.G., Kurz, M.D., 2020. Anomalous ^{182}W in high ^{3}He/^{4}He ocean island Basalts: fingerprints of Earth's core? Geochim. Cosmochim. Acta 271, 194–211. https://doi.org/10.1016/j.gca.2019.12.020.

Ono, S., Wing, B., Johnston, D., Farquhar, J., Rumble, D., 2006. Mass-dependent fractionation of quadruple stable sulfur isotope system as a new tracer of sulfur biogeochemical cycles. Geochim. Cosmochim. Acta 70, 2238–2252.

Rizo, H., Walker, R.J., Carlson, R.W., Horan, M.F., Mukhopadhyay, S., Manthos, V., Francis, D., Jackson, M.G., 2016. Preservation of Earth-forming events in the tungsten isotopic composition of modern flood basalts. Science 80 (352), 809–812. https://doi.org/10.1126/science.aad8563.

Rizo, H., Andrault, D., Bennett, N.R., Humayun, M., Brandon, A., Vlastélic, I., Moine, B., Poirier, A., Bouhifd, M.A., Murphy, D.T., 2019. 182W evidence for core-mantle interaction in the source of mantle plumes. Geochem. Perspect. Lett. 11, 6–11.

Starkey, N.A., Stuart, F.M., Ellam, R.M., Fitton, J.G., Basu, S., Larsen, L.M., 2009. Helium isotopes in early Iceland plume picrites: constraints on the composition of high 3He/4He mantle. Earth Planet. Sci. Lett. 277, 91–100.

Stuart, F.M., Lass-Evans, S., Fitton, J.G., Ellam, R.M., 2003. High 3He/4He ratios in picritic basalts from Baffin Island and the role of a mixed reservoir in mantle plumes. Nature 424, 57.

Thorne, M.S., Garnero, E.J., Jahnke, G., Igel, H., McNamara, A.K., 2013. Mega ultra low velocity zone and mantle flow. Earth Planet. Sci. Lett. 364, 59–67.

Valbracht, P.J., Staudacher, T., Malahoff, A., Allègre, C.J., 1997. Noble gas systematics of deep rift zone glasses from Loihi Seamount, Hawaii. Earth Planet. Sci. Lett. 150, 399–411.

Wicks, J.K., Jackson, J.M., Sturhahn, W., 2010. Very low sound velocities in iron-rich (Mg, Fe) O: implications for the core-mantle boundary region. Geophys. Res. Lett. 37.

Willbold, M., Elliott, T., Moorbath, S., 2011. The tungsten isotopic composition of the Earth's mantle before the terminal bombardment. Nature 477, 195.

Williams, C.D., Mukhopadhyay, S., Rudolph, M.L., Romanowicz, B., 2019. Primitive helium is sourced from seismically slow regions in the lowermost mantle. Geochem. Geophys. Geosyst.

Williams, Q., Garnero, E.J., 1996. Seismic evidence for partial melt at the base of Earth's mantle. Science 273, 1528–1530.

Workman, R.K., Hart, S.R., Jackson, M., Regelous, M., Farley, K.A., Blusztajn, J., Kurz, M., Staudigel, H., 2004. Recycled metasomatized lithosphere as the origin of the Enriched Mantle II (EM2) end-member: evidence from the Samoan Volcanic Chain. Geochem. Geophys. Geosyst. 5, 1–44. https://doi.org/10.1029/2003GC000623.

Workman, R.K., Hauri, E., Hart, S.R., Wang, J., Blusztajn, J., 2006. Volatile and trace elements in basaltic glasses from Samoa: implications for water distribution in the mantle. Earth Planet. Sci. Lett. 241, 932–951. https://doi.org/10.1016/j.epsl.2005.10.028.

Workman, R.K., Eiler, J.M., Hart, S.R., Jackson, M.G., 2008. Oxygen isotopes in Samoan lavas: confirmation of continent recycling. Geology 36, 551–554.

Yuan, K., Romanowicz, B., 2017. Seismic evidence for partial melting at the root of major hot spot plumes. Science 80 (357), 393–397.

Zhang, Z., Dorfman, S.M., Labidi, J., Zhang, S., Li, M., Manga, M., Stixrude, L., McDonough, W.F., Williams, Q., 2016. Primordial metallic melt in the deep mantle. Geophys. Res. Lett. 43, 3693–3699.

Zindler, A., Hart, S.R., 1986. Chemical geodynamics. Annu. Rev. Earth Planet. Sci. 14, 493–571. https://doi.org/10.1146/annurev.earth.14.1.493.